PUNE RESEARCH SCHOLAR ISSN 2455-314X
AN INTERNATIONAL MULTIDISCIPLINARY JOURNAL VOL 3, ISSUE 3

NON-DARCY CONVECTIVE HEAT TRANSFER THROUGH A POROUS MEDIUM IN A CIRCULAR ANNULUS

DR. K. GNANESWAR
Principal,
S.K.P. Government Degree College,
Guntakal, Anantapuramu-Dist. **(AP) INDIA.**

ABSTRACT

We have analyzed the effect of temperature heat source and radiation on mixed convective hydromagnetic flow of a viscous dissipative fluid through a porous medium over cylindrical annulus under radial magnetic field. The equations governing the flow and heat transfer are non-linear and coupled. These equations are solved by using Galerkin finite element method with quadratic interpolation polynomials. The interactions of various forces on the flow and heat transfer characteristics are analyzed. Shear stress, Nusslet number and Grashoff number are evaluated numerically for different values of the governing parameters under consideration and are shown in tabular form

Keywords: *Non-Darcy; Circular annulus; Viscous dissipation; Radiation; Finite element method;*

1 INTRODUCTION

Convective heat transfer in porous media has been studied by scientists and engineers in various disciplines. These include geophysics, hydrology, geothermal operations, heat exchange systems, packed-bed catalytic reactors, insulation engineering and many others. Cheng [5] has reviewed some excellent work resulting from these investigations. Most of the existing analytical studies deal primarily with mathematical simplification based on the Darcy's law, which cannot account for the effects of a solid boundary, inertial forces, and variable porosity on fluid flow and heat transfer through porous media. Boundary effects are expected to become more noticeable when heat transfer is considered in the near-wall region. Inertial effects also become important when fluid velocity is high. Non-Darcian effects i.e., the boundary and inertial effects on heat transfer for constant porosity media were analyzed by Vafai and Tien [17] for forced convection, Kapur & Jain [6, 7] for mixed convection.

Both the boundary and inertia effects decrease fluid velocity in the thermal boundary layer and reduce heat transfer rates.

In almost all these works, the boundary layer formulation of Darcy's law and the energy equation were used. In the Non-Darcian natural convection flow, numerous investigations have been conducted. The inertia effect has been shown to decrease the heat transfer when the Rayleigh number is increased. The buoyancy effect due to a no slip boundary condition also results in a small Nusselt Number but is less pronounced as the Rayleigh number is increased.

Reviews of previous work done on free-convection flow in the annular geometry completely filled with a porous material may be found in several research works. The Binkman flow of a laminar free convection flow in an annular porous region was studied by Sparrow et al [16]. Taking viscous dissipation into account in the energy equation, the free and forced convection flow through a porous medium in a coaxial duct has been analyzed by Vajravelu et al [18]. Beajan et al [3] has analyzed non-Darcy convective heat transfer through a porous medium in a cylindrical annulus with outer cylinder maintained at constant heat flux.

In this chapter we analyze the effect of temperature heat sources and radiation effect on the mixed convective hydro magnetic flow of a viscous dissipative fluid through a porous medium in a cylindrical annulus under a radial magnetic field. The equations governing the flow and heat transfer are non-linear and coupled. These equations are solved by using Galerkin finite element method with quadratic interpolation polynomials. The interactions of various forces on the flow and heat transfer characteristics are analyzed.

2. FORMULATION OF THE PROBLEM

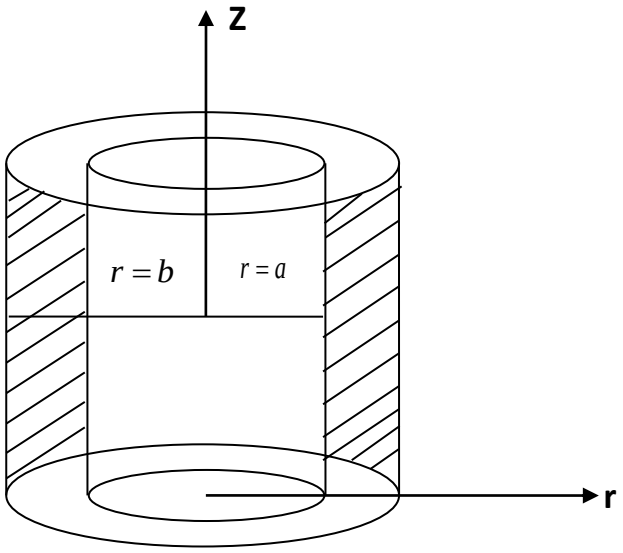

We consider free and forced convection flow in a vertical circular annulus through a porous medium with the inner cylinder maintained at constant temperature and the outer cylinder is maintained at constant heat flux. Also the flow takes place under the uniform axial pressure gradient. The resulting flow is a free and forced convection flow through a porous medium in the coaxial duct. The entire flow region is subjected to the influence of a radial magnetic field. This apart the viscous dissipation is considered in the energy equation and the influence of the viscous dissipation on the flow and heat transfer is being considered.. Both the fluid and porous region have constant physical properties and the flow is a mixed convection flow taking place under thermal buoyancy and uniform axial pressure gradient. The Brinkman-Forchheimer Extended Darcy model which accounts for the inertia and boundary effects has been used for the momentum equation in the porous region. Here, the thermo physical properties of the solid and fluid have been assumed to be constant except for the density variation in the body force term (Bossiness approximation), and the solid particles and fluid are considered to be in local thermal equilibrium. In the absence of any extraneous forces the flow is unidirectional along the axis of the duct assumed to be of infinite span.

The Brinkman-Forchhemer - extended Darcy equation which account for boundary inertia effects in the momentum equation is used to obtain the velocity field, Based on the above assumptions the governing equations in the vector form are

Equation of continuity

$$\nabla \cdot \bar{q} = 0 \tag{2.1}$$

Equation of linear momentum

$$\frac{\rho}{\delta}\frac{\partial \bar{q}}{\partial t} + \frac{\rho}{\delta^2}(\bar{q}\cdot\nabla)\bar{q} = -\nabla p + \rho g - \left(\frac{\mu}{k}\right)\bar{q} - \frac{\rho F}{\sqrt{k}}\bar{q}\,\bar{q} + \mu\nabla^2\bar{q} \tag{2.2}$$

Equation of Energy

$$\rho C_p\left(\frac{\partial T}{\partial t} + (\bar{q}\cdot\nabla)T\right) = \lambda\nabla^2 T + Q \tag{2.3}$$

Equation of State

$$\rho - \rho_0 = -\beta g(T - T_0) \tag{2.4}$$

where $\bar{q} = (0,0,u)$ is the velocity, T is the temperature of the fluid, p is the pressure, ρ is the density of the fluid, C_p is the specific heat at constant pressure, k is the permeability of the porous medium, μ is the coefficient of viscosity of fluid, δ is the porosity of the medium, β is the coefficient of thermal expansion, λ is coefficient of thermal conductivity, σ is the

electrical conductivity and μ_e is the permeability of the medium, Q is the strength of the heat sources and F is the function that depends on the Reynolds number and the microstructure of porous medium. Here the physical properties of the solid and the fluid state have been assumed to be constant except for the density variation in the body force term (Boussinesq approximation) and the solid particles and the fluid are considered to be in local thermal equilibrium.

Since the flow is unidirectional, the equation of continuity reduces to $\frac{\partial u}{\partial z} = 0$. where 'u' is the axial velocity implies u= u(r). Also the flow is in unidirectional along the axial cylindrical annulus. Making use of the above assumptions the governing equations are

$$\frac{-\partial p}{\partial z} + \frac{\mu}{\delta}\left(\frac{\partial^2 u}{\partial r^2} + \frac{1}{r}\frac{\partial u}{\partial r}\right) - \frac{\mu}{k}u - \frac{\rho\delta F}{\sqrt{k}}u^2 + \rho g(T - T_0)\beta - \frac{\sigma\mu^2 H_0^2}{r^2}u = 0 \tag{2.5}$$

The equation of the energy which accounts for viscous dissipation is

$$\rho c_\rho u\frac{\partial T}{\partial z} = \left(\frac{\partial^2 T}{\partial r^2} + \frac{1}{r}\frac{\partial T}{\partial r}\right) + \mu\left(\frac{\partial u}{\partial r}\right)^2 + Q \tag{2.6}$$

The equation of continuity in view of the unidirectional flow reduces to $\frac{\partial u}{\partial r} = 0$
Implies u = u(r), where u is the velocity component along axial direction,
The boundary conditions are

u(a) = 0 =u(b) (2.7)

and T(a) = T_0, $\left(\frac{\partial T}{\partial r}\right)_{r=b} = Q$ (constant heat flux) (2.8)

The axial temperature gradient $\frac{\partial T}{\partial z}$ assumed to be a constant by A. We define the following non-dimensional variables

$$z^* = \frac{z}{a},\quad r^* = \frac{r}{a},\quad u^* = \frac{au}{\gamma},\quad p^* = \frac{pa^2\delta}{\rho\gamma^2},\quad \theta^* = \frac{T - T_0}{Aa},\quad Q^* = \frac{Q}{A},\quad s^* = \frac{b}{a}.$$

Introducing these non-dimensional variables then the governing equations in the non-dimensional form reduce to (on dropping the stars)

$$\frac{\partial^2 u}{\partial r^2}+\frac{1}{r}\frac{\partial u}{\partial r}=\pi+\delta D^{-1}u+\delta^2\wedge u^2-\delta G(\theta)-\frac{\delta M^2 u}{r^2} \qquad (2.9)$$

$$\frac{\partial^2 \theta}{\partial r^2}+\frac{1}{r}\frac{\partial \theta}{\partial r}+\alpha=N_T Pu-P_1 E_c\left(\frac{\partial u}{\partial r}\right)^2 \qquad (2.10)$$

where

$\wedge = FD^{-½}$ (Inertia parameter or Furchheimer Number)

$G=\frac{g\beta(Aa)a^3}{\gamma^2}$ (Grashoff number)

$D^{-1}=\frac{a^2}{K}$ (Inverse Darcy parameter)

$E_c=\frac{\gamma^2}{a^2(Aa)c_p}$ (Eckert number)

$P_1=\frac{\mu C_p}{\lambda},$ (Prandtl number)

$M^2=\frac{\sigma\mu_e^2 H_0^2 a^2}{\gamma^2}$ (Hartman number)

$N=\frac{Aa}{T_i-T_0}$ (non-dimensional temperature gradient)

The corresponding boundary conditions are

$u(1)=u(s)=0,\ \theta(1)=0,\ \left(\frac{d\theta}{dr}\right)_{r=s}=Q_1$ (non-dimensional constant heat flux)

The shear stress are evaluated on the cylinder using the formula

$$\tau=\left(\frac{du}{dr}\right)_{r=1+s}$$

The rate of heat transfer (Nusselt number) is evaluated on the cylinder using the formula

$$Nu=-\left(\frac{d\theta}{dr}\right)_{r=1+s}$$

3. FINITE ELEMENT ANALYSIS

The finite-element method (FEM) is such a powerful method for solving ordinary differential equations and partial differential equations. The basic idea of this method is dividing the whole domain into smaller elements of finite dimensions called finite elements. This method is such a good numerical method in modern engineering analysis, and it can be applied for solving integral equations including heat transfer, fluid mechanics, chemical processing, electrical systems, and many other fields. The steps involved in the finite-element are as follows.

(i) Finite-element discretization.
(ii) Generation of the element equations.
(iii) Assembly of element equations.
(iv) Imposition of boundary conditions.
(v) Solution of assembled equations.

The assembled equations so obtained can be solved by any of the numerical techniques, namely, the Gauss elimination method, LU decomposition method, etc. An important consideration is that of the shape functions which are employed to approximate actual functions.

4. Results and Discussion

In this analysis we investigate non-Darcy convective heat transfer through a porous medium confined in a cylindrical annulus with the outer wall maintained at constant heat flux and the inner wall at constant temperature. The non-linear equations governing the flow and heat transfer have been solved by using Galerkine finite element technique. The velocity, the temperature, the stress (τ) and Nusselt number (Nu) have been calculated for different sets of parameters, viz G, M, D^{-1} and α in two cases viz., wide gap and narrow gap. The velocity w is exhibited in figures 1 - 4 in wide gap case and 9-12 in narrow gap case. The axial velocity is in the vertically downward direction and hence w > 0 represents the reversal flow. Figure 1 & 9 represents the axial velocity w with Grashoff number G. It is found that both in wide and narrow gap cases the velocity changes from negative to positive as we move from the inner to the outer cylinder there by indicating the reversal flow in the region adjacent to outer cylinder while for G <0 the reversal flow occurs in the vicinity of the inner cylinder. The region of reversal flow enlarges with increasing |G|. The magnitude of w enhances with |G| in wide gap case while in a narrow gap case |w| reduces with increase in $|G| \leq 3\times10^3$ and enhances with higher $|G| \geq 5\times10^3$ the maximum occurs at r =1.2 in both the cases. The variation of w with D^{-1} shows that lesser the permeability of the porous medium smaller |w|

in both the cases (fig 3 & 11). Figures 2 & 10 represent the variation of w with Hartman number M. It is found that higher the Lorentz force smaller the magnitude of w in the flow region. The variation of w with heat source parameter α shows that an increase in the strength of heat source/sink enhances |w|. Also it is found that in wide gap case the reversal flow which appears in the vicinity at r = 2 disappear for higher α >0 while for α <0 we notice the reversal flow in the entire flow region. In narrow gap case for all values of $|\alpha|$ we find reversal flow in the vicinity of outer cylinder and its size enlarges with α <0 in wide gap case while in narrow gap its size reduces with α >0 and enlarges with α <0 (fig 4 & 12).

The non-dimensional temperature distribution (θ) is exhibited in figs 5 - 8 in wide gap case while in figs 13 - 16 in narrow gap case. It is found that the temperature is positive for all variations in $G, M, D^{-1}, \alpha > 0$ and negative in for all α <0. It is found that the temperature θ enhances with |G| in wide gap case while in narrow gap case the temperature enhances in the flow region for G>0 while for G<0, θ enhances except in the vicinity of the outer cylinder(fig 5 & 13). The variation of θ with D^{-1} exhibits that lesser the permeability of the porous medium larger the temperature in a wide gap case and smaller the temperature in narrow gap case (fig 7 & 15). From figs 6 & 14 we find that the temperature depreciates in the flow region in both wide and narrow gap cases. The variation of θ with α is exhibited in figs 8 & 16. It is found that an increase in the strength of a heat source/sink leads to an enhancement in the temperature in both wide and narrow gap cases.

The shear stress τ at the inner and outer cylinders have been evaluated for the different values of G, M, D^{-1}, and α are represented in tables 1-16. It is found that the stress at r = 1 is negative for G>0 and positive for G<0. An increase in |G| enhances $|\tau|$ and an increase in M or D^{-1} depreciates $|\tau|$ at r = 1 in both the cases. Also $|\tau|$ enhances with α >0 and reduces with α <0 in both wide and narrow gap cases (table 1, 2, 7 and 8). The shear stress at the outer cylinder enhances with increase |G| in wide gap case while in narrow gap case it reduces with $|G| \leq 3\times10^3$ and enhances with $|G| \geq 5\times10^3$. The variation of τ with D^{-1} shows that lesser the permeability of porous medium smaller $|\tau|$ in wide gap case and larger $|\tau|$ in narrow gap case. Also higher the Lorentz force larger $|\tau|$ at the outer cylinder in both narrow and wide gap cases. An increase in the strength of heat source (α >0) enhances $|\tau|$ in wide gap cases and depreciates in narrow gap case while an increase α <0 enhances $|\tau|$ in both the cases (tables 3, 4, 9 and 10). In general we notice that the shear stress in wide gap case is smaller compared to that in narrow gap case.

The rate of heat transfer at the inner cylinder has been calculated for different G, M, D^{-1}, and α are represented in tables 5 & 6 in wide gap case in tables 11 & 12 in narrow gap case. It is found that the rate of heat transfer is negative at the inner cylinder for all variations. An increase in |G| reduces the rate of heat transfer at r = 1. The variation of Nu with D^{-1} reveals that lesser the permeability of porous medium smaller |Nu| in both the cases. Also higher the Lorentz force smaller the rate of heat transfer in wide gap case and larger |Nu| in narrow gap case. In wide gap case an increase in the strength of heat source $\alpha \leq 4$ reduces the rate of heat transfer and for higher $\alpha \geq 6$, we notice an enhancement |Nu| while in narrow gap case it reduces while $\alpha \geq 0$. An increase with $\alpha < 0$ enhances the rate of heat transfer at the inner cylinder in both the cases (tables 5, 6, 11 & 12).

REFERENCES

1	Basant Kumar Jha	"Free convection flow through annular porous medium", Heat Mass Transfer,41,pp.675-679	2005
2	Bejan,A,Tien,C.L	"Natural convection in a horizontal space bounded by the two convective cylinders with different end temperatures", Int.J.Heat Mass transfer 29,pp.1513-1519	1986
3	Bejan, A and Poulikakos, A	"The Non-Darcy regimes for vertical boundary layer natural convection in a porous media", Int.J.Heat Mass Transfer,27,pp.717 - 722	1984
4	Cha-O-Kaung Chen & Chien-Hsinchen	"Non-uniform porosity and Non-Darcian effects on conjugate mixed convection heat transfer from a plate filled in porous media",Vol.11.pp.65-71	1990
5	Cheng,P	"Heat transfer in geothermal systems", Adv. Heat transfer 14,pp.1- 105	1978
6	Kapur,J.N&Jain,R.K	"Physics of Fluids3", p.664	1960
7	Kapur,J.N&Jain ,R.K	"Mathematics Seminar2",p.205	1962
8	Kou,J.N,Lu,K.T	"Combined boundary and inertial effects of fully developed mixed convection in a vertical channel embedded in porous media",Int.Commun Heat Mass Transfer20,pp.333-345	1993

9	Oreper,G.M,Szekely	"The effect of an externally imposed magnetic field on buoyancy driven flow in a rectangular cavity", J.cryst.Growth64,pp.505-515	1983
10	Ozoe,H, Maruo,M	"Magnetic and gravitational natural convection of melted silicon-two dimensional numerical computations for the rate of heat transfer",JSME30,pp.774-784	1987
11	Pai,S.I	"JournalofAppl.Phys.25",p.1205	1954
12	Poots,G	"Int. Journal of Heat Mass Transfer",3,p.1	1961
13	Prasad,V	"Natural convection in porous media",Ph.D Thesis, S.V.University	1983
14	Riley,N	"Magneto hydrodynamic convection", J.FluidMech18,pp.577-586	1964
15	Sarojamma,G	"Magneto hydrodynamic convection flow", Ph.D Thesis, S.K.University	1981

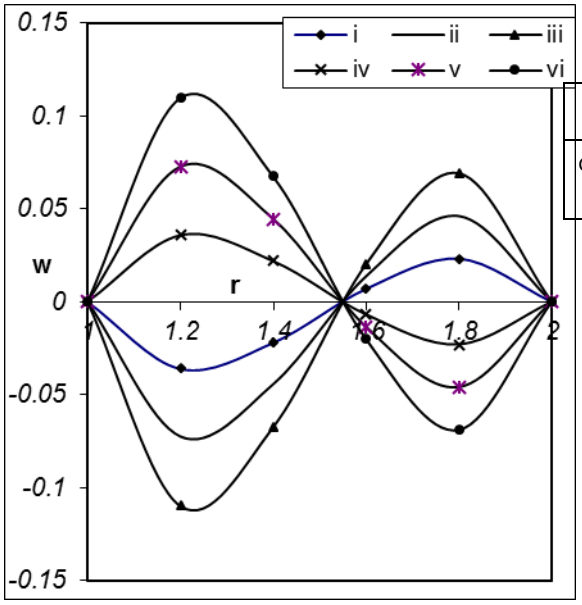

$M = 2,\ D^{-1} = 10^3,\ \alpha = 2,\ N = 1$

	i	ii	iii	iv	v	vi
G	10^3	3×10^3	5×10^3	-10^3	-3×10^3	-5×10^3

Figure 1. Velocity w with G

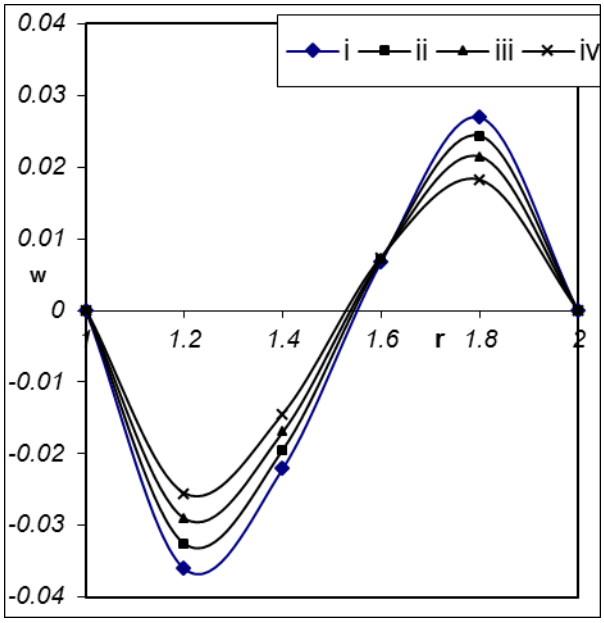

Figure 2. Velocity w with M

$G = 10^3$, $D^{-1}=10^3$, α =2, N=1

	i	ii	iii	iv
M	2	3	4	5

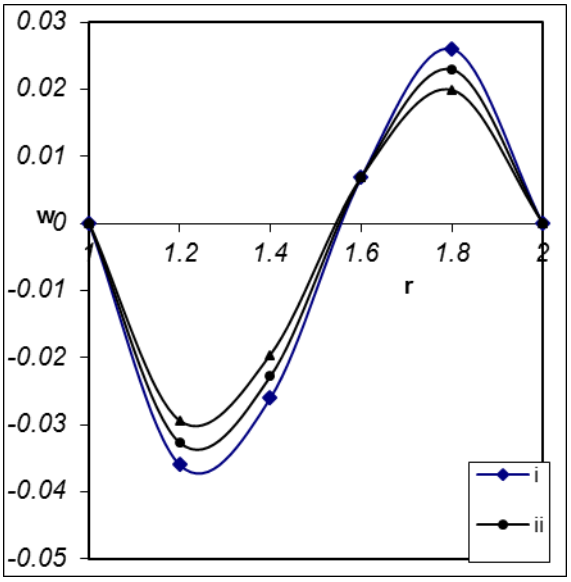

Figure 3. Velocity w with D^{-1}

M = 2, $G=10^3$, α =2, N=1

	i	ii	iii
D^{-1}	10^3	2×10^3	3×10^3

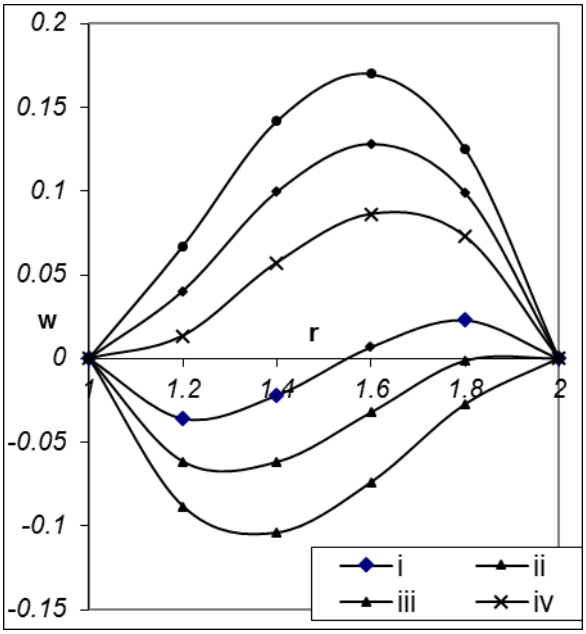

Figure 4. Velocity w with α

M = 2, $G=10^3$, $D^{-1}=10^3$, N=1

	i	ii	iii	iv	v	vi
α	2	4	6	-2	-4	-6

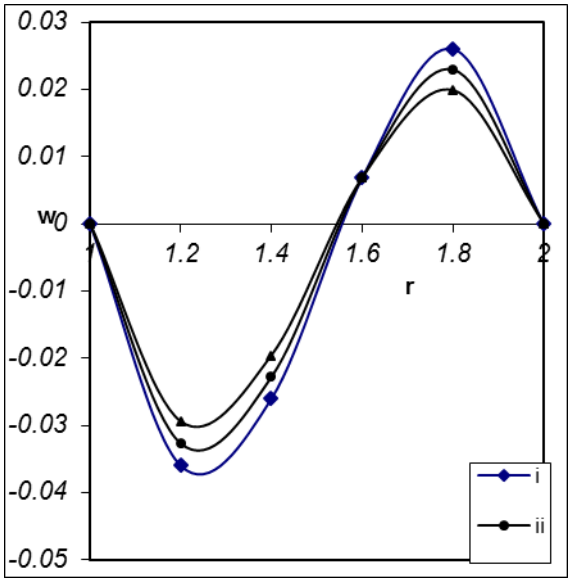

Figure 5. Velocity w with D^{-1}

M = 2, G=10^3 , α =2, N=1

	i	ii	iii
D^{-1}	10^3	2×10^3	3×10^3

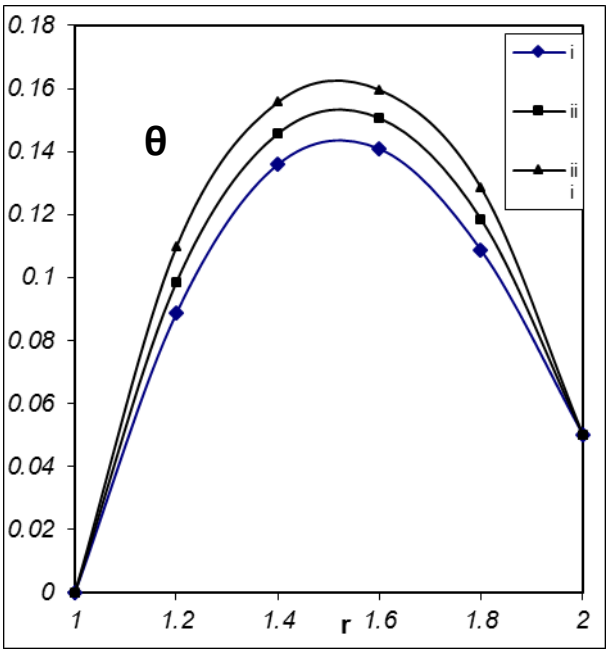

Figure 7. Temperature θ with D^{-1}

M = 2, G=10^3 , α =2, N=1

	i	ii	iii
D^{-1}	10^3	2×10^3	3×10^3

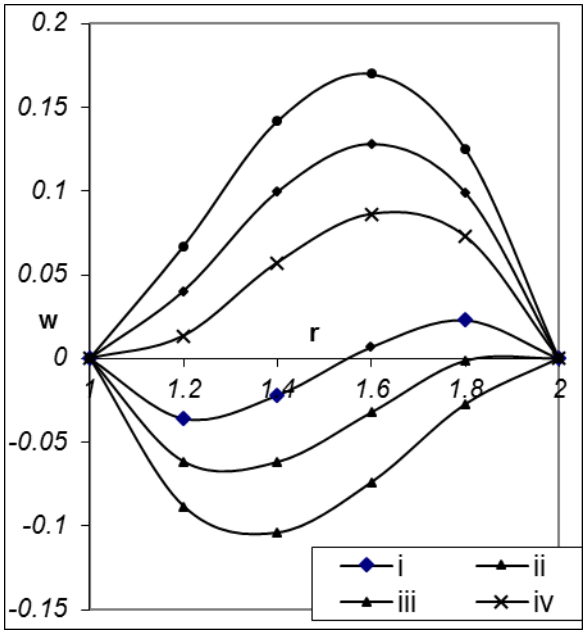

Figure 6. Velocity w with α

M = 2, G=10^3 , D^{-1}=10^3, N=1

	i	ii	iii	iv	v	vi
α	2	4	6	-2	-4	-6

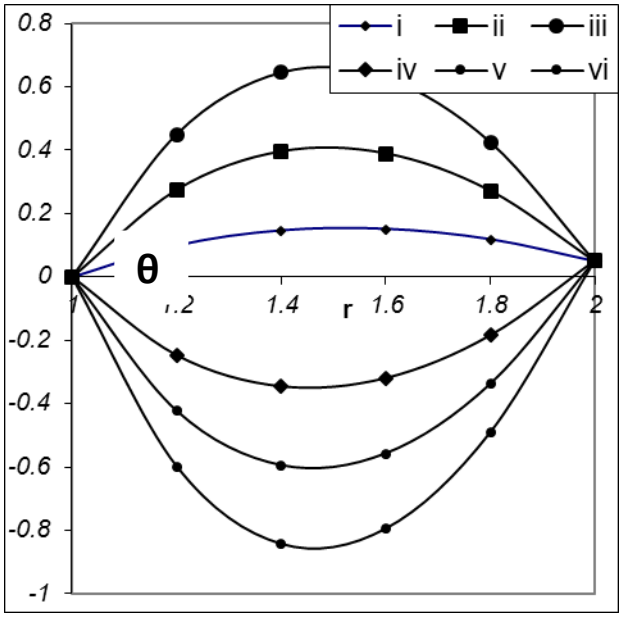

Figure 8. Temperature θ with α

M = 2, G=10^3, D^{-1}=10^3, N=1

	i	ii	iii	iv	v	vi
α	2	4	6	-2	-4	-6

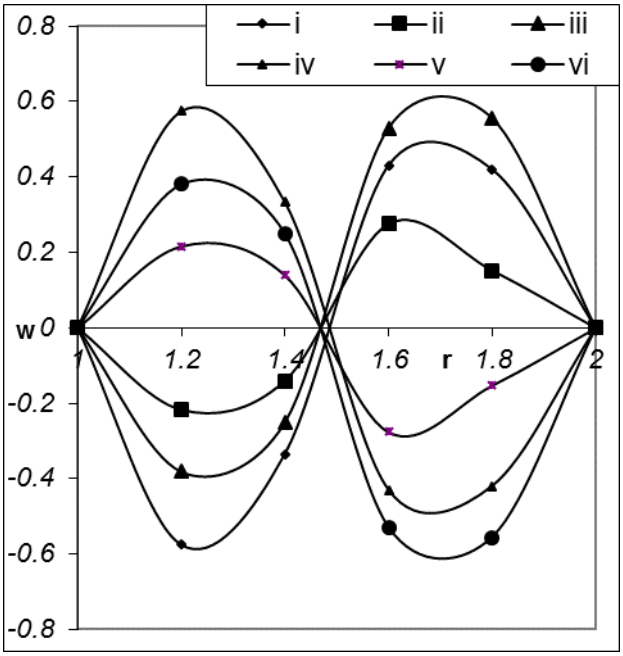

Figure 9. Velocity w with G

M = 2, D^{-1}=10^3, α =2, N=1

	i	ii	iii	iv	v
G	10^3	3×10^3	5×10^3	-10^3	-3×10^3

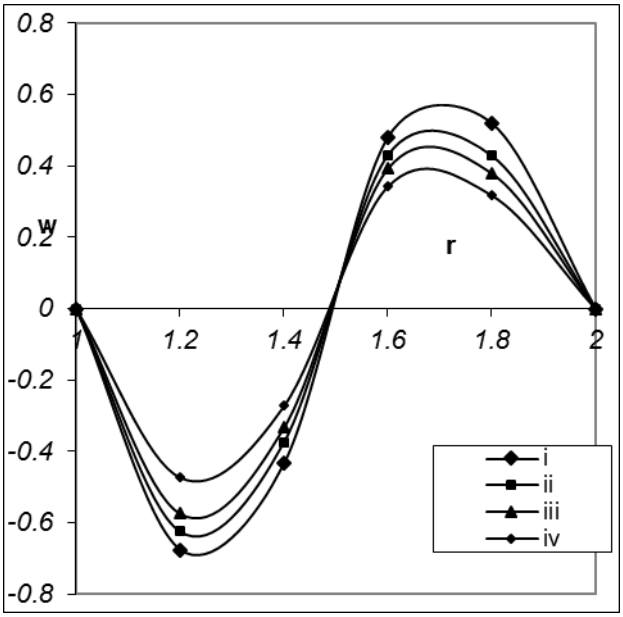

Figure 10. Velocity w with M

G = 10^3, D^{-1}=10^3, α =2, N=1

	i	ii	iii	iv
M	2	3	4	5

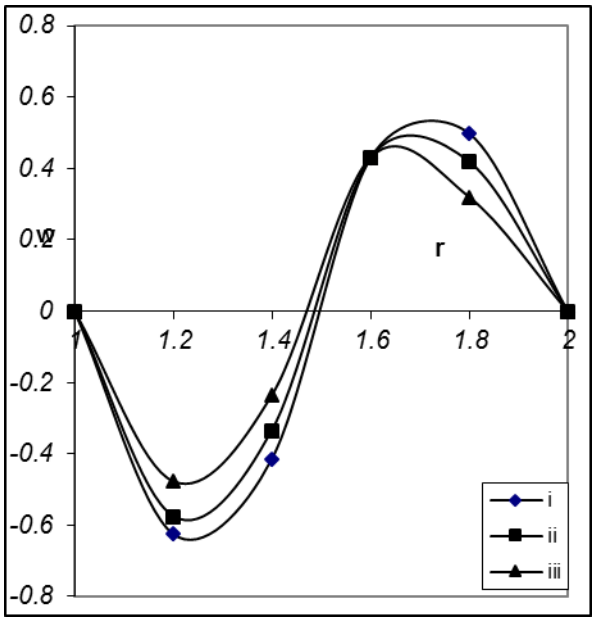

Figure 11. Velocity W with D^{-1}

M = 2, G=10^3 , α =2, N=1

	i	ii	iii
D^{-1}	10^3	2×10^3	3×10^3

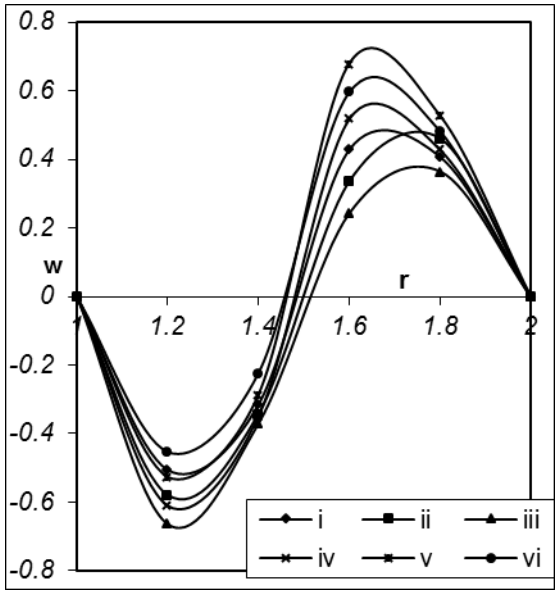

Figure 12. Velocity W with α

M = 2, G=10^3 , D^{-1}=10^3, N=1

	i	ii	iii	iv	v	vi
α	2	4	6	-2	-4	-6

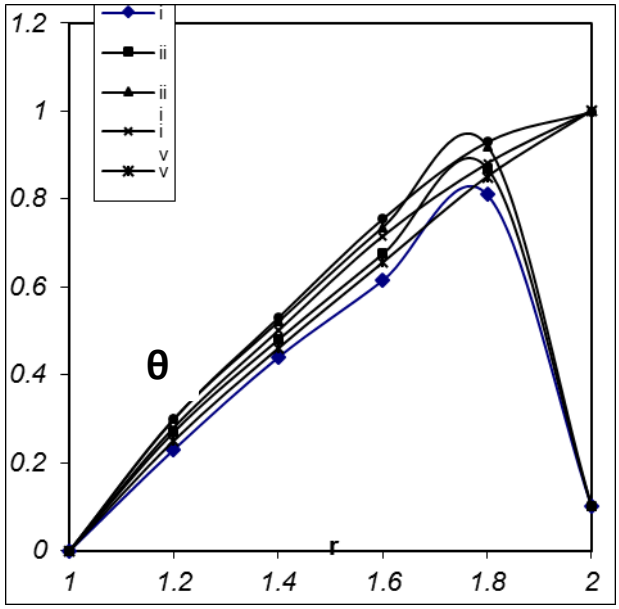

Figure 13. Temperature θ with G

M = 2, D^{-1}=10^3, α =2, N=1

	i	ii	iii	iv	v	vi

G	10^3	3×10^3	5×10^3	-10^3	-3×10^3	-5×10^3

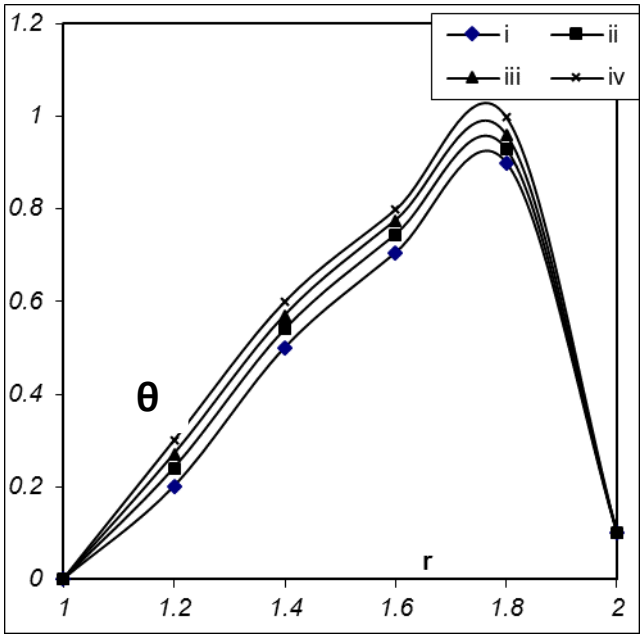

Figure 14. Temperature θ with M

$G = 10^3$, $D^{-1}=10^3$, α =2, N=1

	i	ii	iii	iv
M	2	3	4	5

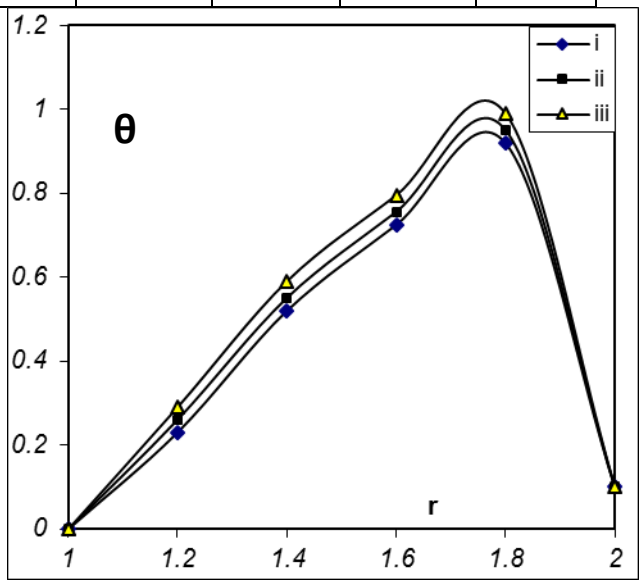

Figure 15 Temperature θ with D^{-1}

M = 2, $G=10^3$, α =2, N=1

	i	ii	iii
D^{-1}	10^3	2×10^3	3×10^3

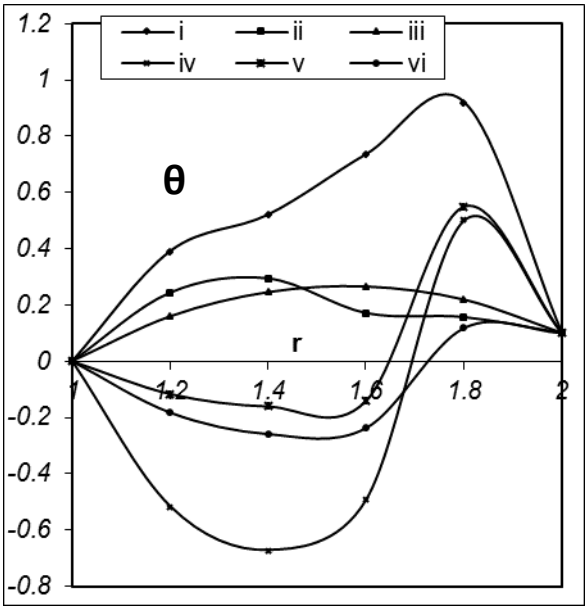

Figure 16. Temperature θ with α

M = 2, $G=10^3$, $D^{-1}=10^3$, N=1

	i	ii	iii	iv	v	vi
α	2	4	6	-2	-4	-6

Table – 1

Shear stress $[\tau]_{r=1}$ *at* $s=1$ (*wide gap case*), $\alpha=2,\ N=1$

G	i	ii	iii	iv	v
10^3	-0.88945	-0.7799	-0.58078	-0.88511	-0.87735
3×10^3	-1.79112	-1.57034	-1.16782	-1.78321	-1.76771
5×10^3	-2.69307	-2.36083	-1.75536	-2.68148	-2.65874
-10^3	0.88945	0.7799	0.58078	0.88511	0.87735
-3×10^3	1.79111	1.57033	1.16782	1.78318	1.76764
-5×10^3	2.69269	2.36076	1.7549	2.68025	2.65568
M	2	3	5	2	2
D^{-1}	10^3	10^3	10^3	3×10^3	5×10^3

Table - 2

Shear stress $[\tau]_{r=1}$ *at* $s=1$ (*wide gap case*), $M=2,\ D^{-1}=10^3, N=1$

G	i	ii	iii	iv	v	vi
10^3	-0.88945	-1.03458	-1.18075	-0.59916	-0.48202	-0.33618
3×10^3	-1.79112	-2.0828	-2.3742	-1.20866	-0.95203	-0.66066
5×10^3	-2.69307	-3.13028	-3.56697	-1.82018	-1.42439	-0.98832
-10^3	0.88945	1.03458	1.18074	0.59916	0.48201	0.33617
-3×10^3	1.79111	2.08243	2.37328	1.20859	0.95205	0.66076
-5×10^3	2.69269	3.12766	3.56238	1.81988	1.4243	0.98822
α	2	4	6	-2	-4	-6

Table - 3

Shear stress $[\tau]_{r=1+s}$ *at* $s=1$ (*wide gap case*), $\alpha=2, N=1$

G	i	ii	iii	iv	v
10^3	0.00882	-0.02985	-0.08504	0.00665	0.00291
3×10^3	0.02527	-0.05289	-0.16579	0.02142	0.01393
5×10^3	0.04193	-0.07582	-0.24585	0.03677	0.02671
-10^3	-0.00881	0.02985	0.08503	-0.00665	-0.00291
-3×10^3	-0.02525	0.0529	0.16577	-0.02136	-0.01381
-5×10^3	-0.04128	0.07594	0.24634	-0.0346	-0.02152
M	2	3	5	2	2
D^{-1}	10^3	10^3	10^3	3×10^3	5×10^3

Table - 4

Shear stress $[\tau]_{r=1+s}$ *at* $s=1$ (*wide gap case*), $M=2,\ D^{-1}=10^3, N=1$

G	i	ii	iii	iv	v	vi
10^3	0.00882	0.15447	0.30077	-0.27894	-0.40924	-0.55544

3×10^3	0.02527	0.3174	0.60926	-0.55607	-0.82517	-1.11672
5×10^3	0.04193	0.4797	0.91684	-0.82926	-1.23683	-1.67238
-10^3	-0.00881	-0.15445	-0.30073	0.27891	0.40919	0.55537
-3×10^3	-0.02525	-0.31667	-0.60748	0.55599	0.82482	1.11619
-5×10^3	-0.04128	-0.47511	-0.90868	0.82962	1.23667	1.6722
α	2	4	6	-2	-4	-6

Table - 5

Nusselt Number $[Nu]_{r=1}$ *at* $s=1$ (*wide gap case*), $\alpha=2,\ N=1$

G	i	ii	iii	iv	v
10^3	-0.81827	-0.81826	-0.81826	-0.81824	-0.81816
3×10^3	-0.81801	-0.81801	-0.81802	-0.81775	-0.81724
5×10^3	-0.81735	-0.81743	-0.81719	-0.81616	-0.81383
-10^3	-0.81827	-0.81826	-0.81826	-0.81824	-0.81817
-3×10^3	-0.81801	-0.81809	-0.81827	-0.81779	-0.81737
-5×10^3	-0.8178	-0.81767	-0.81775	-0.81792	-0.81882
M	2	3	5	2	2
D^{-1}	10^3	10^3	10^3	3×10^3	5×10^3

Table – 6

Nusselt Number $[Nu]_{r=1}$ *at* $s=1$ (*wide gap case*), $M=2,\ D^{-1}=10^3, N=1$

G	i	ii	iii	iv	v	vi
10^3	-0.81827	0.2778	1.37407	-3.0117	-4.07479	-5.17135
3×10^3	-0.81801	0.27808	1.37399	-3.01004	-4.07202	-5.16725
5×10^3	-0.81735	0.27845	1.37408	-3.0062	-4.06677	-5.16045
-10^3	-0.81827	0.2778	1.37417	-3.01181	-4.07507	-5.17189
-3×10^3	-0.81801	0.27757	1.37282	-3.01091	-4.07331	-5.16918
-5×10^3	-0.8178	0.27561	1.36919	-3.00838	-1.06962	-5.16458
α	2	4	6	-2	-4	-6

Table – 7

Shear stress $[\tau]_{r=1}$ *at* $s=0.2$ (*narrow gap case*), $\alpha=2, N=1$

G	i	ii	iii	iv	v
10^3	-0.13184	-0.13148	-0.13031	-0.13182	-0.13178
3×10^3	-0.33297	-0.33136	-0.32249	-0.33294	-0.33287
5×10^3	-0.53701	-0.53379	-0.51672	-0.53693	-0.53679
-10^3	0.13184	0.13148	0.13031	0.13184	0.13182
-3×10^3	0.33297	0.33136	0.32249	0.33294	0.33287
-5×10^3	0.53701	0.53379	0.51672	0.53693	0.53679
M	2	3	5	2	2
D^{-1}	10^3	10^3	10^3	3×10^3	5×10^3

Table – 8

Shear stress $[\tau]_{r=1}$ *at* $s = 0.2$ (*narrow gap case*), $M = 2$, $D^{-1} = 10^3, N = 1$

G	i	ii	iii	iv	v	vi
10^3	-0.13184	-0.13466	-0.13506	-0.13109	-0.13071	-0.13033
3×10^3	-0.33297	-0.33639	-0.3398	-0.3281	-0.32668	-0.32327
5×10^3	-0.53701	-0.5715	0.5442	-0.53165	-0.52535	-0.52273
-10^3	0.13184	0.13466	0.13506	0.13109	0.13071	0.13033
-3×10^3	0.33297	0.33639	0.3398	0.3281	0.32668	0.32327
-5×10^3	0.53701	0.5415	0.5442	0.53165	0.52535	0.52273
α	2	4	6	-2	-4	-6

Table – 9

Shear stress $[\tau]_{r=1+s}$ *at* $s = 0.2$ (*narrow gap case*), $\alpha = 2, N = 1$

G	i	ii	iii	iv	v
10^3	-0.01622	-0.01628	-0.01646	-0.01622	-0.01623
3×10^3	-0.00064	-0.00126	-0.00551	-0.00066	-0.00068
5×10^3	0.02411	0.12258	0.013	0.02408	0.024
-10^3	0.01622	0.01628	0.01646	0.01622	0.01623
-3×10^3	0.00064	0.00126	0.00551	0.00066	0.00068
-5×10^3	-0.02411	-0.02258	-0.013	-0.2408	-0.024
M	2	3	5	2	2
D^{-1}	10^3	10^3	10^3	3×10^3	5×10^3

Table – 10

Shear stress $[\tau]_{r=1+s}$ *at* $s = 0.2$ (*narrow gap case*), $M = 2$, $D^{-1} = 10^3, N = 1$

G	i	ii	iii	iv	v	vi
10^3	-0.01622	-0.01475	-0.01404	-0.01762	-0.01832	-0.01902
3×10^3	-0.00064	0.00259	0.00585	-0.00585	-0.00783	-0.011
5×10^3	0.02411	0.02878	0.03219	0.01733	0.0114	0.00804
-10^3	0.01622	0.01475	0.01404	0.01762	0.01832	0.01902
-3×10^3	0.00064	-0.00259	-0.00585	0.00585	0.00783	0.011
-5×10^3	-0.02411	-0.02878	-0.03219	-0.01733	-0.0114	-0.00804
α	2	4	6	-2	-4	-6

Table – 11

Nusselt Number $[Nu]_{r=1}$ *at* $s = 0.2$ (*narrow gap case*), $\alpha = 2$, $N = 1$

G	i	ii	iii	iv	v
10^3	-5.37565	-5.37575	-5.37585	-5.37560	-5.37555
3×10^3	-5.37560	-5.37555	-5.37575	-5.37555	-5.37550
5×10^3	-5.37555	-5.37560	-5.37565	-5.37550	-5.37545
-10^3	-5.37550	-5.37555	-5.37560	-5.37545	-5.37540
-3×10^3	-5.37545	-5.37550	-5.37555	-5.37540	-5.37535

-5×10^3	-5.37540	-5.37545	-5.37550	-5.37535	-5.37530
M	2	3	5	2	2
D^{-1}	10^3	10^3	10^3	3×10^3	5×10^3

Table – 12

Nusselt Number $[Nu]_{r=1}$ *at* $s=0.2$ (*narrow gap case*), $M=2,\ D^{-1}=10^3, N=1$

G	i	ii	iii	iv	v	vi
10^3	-5.37565	-5.18120	-4.98484	-5.76823	-5.96449	-6.16071
3×10^3	-5.37560	-5.18110	-4.98474	-5.76813	-5.96449	-6.16061
5×10^3	-5.37555	-5.18102	-4.98464	-5.76803	-5.96429	-6.16051
-10^3	-5.37568	-5.18122	-4.98484	-5.76826	-5.96452	-6.16074
-3×10^3	-5.37562	-5.18112	-4.98474	-5.76816	-5.96442	-6.16059
-5×10^3	-5.37558	-5.18100	-4.98464	-5.76806	-5.96432	-6.16046
α	2	4	6	-2	-4	-6